This manuscript is accepted for publication in Applied Thermal Engineering

A macroscopic particle modelling approach for non-isothermal solid-gas and solid-liquid flows through porous media

Andrea Robone[1], Sahan Trushad Wickramasooriya Kuruneru[2], Mohammad Saidul Islam[3], Suvash Chandra Saha[3]*

[1]Dipartimento di Architettura e Ingegneria, Università degli studi di Parma, Parma, Italy
[2]School of Physics, Chemistry & Mechanical Engineering, Queensland University of Technology, Brisbane, Australia
[3]School of Mechanical and Mechatronic Engineering, Faculty of Engineering and Information Technology, University of Technology Sydney, Ultimo NSW 2007, Australia

*Corresponding author email address: Suvash.Saha@uts.edu.au

Abstract

The complexity of multiphase flows in many engineering systems such as heat exchangers signify the need to develop new and advanced numerical models to analyse the interactions the working fluid and unwanted solid foulants. Fouling is present in a myriad of industrial and domestic processes and it has a negative impact on the economy and the environment. The mechanisms that govern non-isothermal solid-fluid flow through porous metal foam heat exchangers are complex and poorly understood. In this research, a coupled finite volume method (FVM) and macroscopic particle model (MPM) is developed and implemented in ANSYS Fluent to examine the transient evolution of a non-isothermal multiphase solid-fluid flow and the interaction between coupled interactions of solid particles, fluid, and porous media. The maximum particle temperature is dependent on the fluid and solid particle thermo-physical properties in addition to the temperature of the cylindrical ligaments of the porous media. The present results show that the smallest solid particles reach the highest temperatures in the porous heat exchanger and at low inlet velocities, the highest particle temperatures are realized. The results pertaining to maximum particle temperatures are prevalent in many industrial processes and acquiring knowledge of the maximum particle temperature serves as a steppingstone for comprehending complex multiphase solid-fluid flows such as the cohesiveness between the particles and the particle adhesion with the walls. The results of these studies could potentially be used in the future to optimize metal foam heat exchanger designs.

Keywords

Metal Foam; Macroscopic Particle Model; Heat Exchanger Fouling; Heat Transfer; Porous Media.

1. Introduction

Heat exchangers allow the exchange of heat between two fluids that have different temperatures and these fluids are separated by a solid wall. The transfer of heat is encountered in a myriad of industrial and domestic processes in the form of heat exchangers. Heat exchangers are omnipresent in many industries such as power generation, energy generation, food industry, chemical, pharmaceutical, electronics, among others. In particular, heat exchangers are present in commercial and residential buildings in the form of heating, ventilation, air-conditioning and refrigeration systems (HVAC&R), in addition to engines, turbines and compressors, and even in waste heat recovery systems. Clearly, heat exchangers are used in many industrial applications and it is very important to study the heat exchanger performance with the overarching goal of optimizing the thermal performance and efficiency of heat exchangers. Engineers and scientists continue to work on devising methods and strategies to reduce the operational costs and also to increase the thermal performance and efficiency of heat exchangers. As such, the heat exchanger market is continuously increasing and according to the published literature, the heat exchanger market will reach US $78 billion by 2020 (Acmite 2013). Moreover, the global energy demand will increase by 35% over the next two decades; however, this can be as high as 95% in the event energy efficient technologies are not utilized (Ammar 2012). As such, it is of paramount importance to devise innovative, economical, and efficient heat exchanger technologies. In this regard, the use of open-cell porous metal foams are seen as an attractive and viable alternative to traditional fin heat exchangers.

Metal foam is a cellular structure and it comprises a solid metal that usually is aluminium or copper with fluid-filled pores that occupy a large part of the volume. Metal foam is a class of highly porous media and it has a very large surface area to volume ratio and low weight thereby making it attractive for lightweight and compact heat exchangers such as electronics cooling. Furthermore, metal foam is not flammable and metal foams are eco-friendly because they are recyclable and they have very good noise attenuation properties. The pores of a metal foam can be sealed or interconnected and to recognize this distinction the metal foam is called respectively closed-cell foam or open-cell foam. In the closed-cell foam the dimension of the pores is usually between 1-8 mm and this kind of metal foam is usually used as material to absorb large and violent impacts and must be changed after one large impact because the metal foam

becomes deformed. The commercial production of closed-cell metal foams began in the 1990 thanks to a Japanese company and this foam can be made by injecting gas into the liquid metal or causing gas formation in the liquid by admixing gas-releasing blowing agents with the molten metal or causing the precipitation of gas that was previously dissolved in the molten metal (Banhart 2000). Open-cell foams have a stochastic and irregular structure connected by metal ligaments and the 3D geometry of a singular cell could be considered similar to the Weaire-Phelan structure (Bock & Jacobi 2013). Open-cell foam is product by foundry or powder metallurgy using space holders to occupy the pore spaces and channels and for his high cost it is used just for very specific applications like heat exchangers due to its large specific surface area to volume ratio and high porosity. It is worth mentioning that open-cell metal foams have two important parameters to recognize the geometric morphology of metal foam. The first one is the number of pores per inch (PPI) and the second is the porosity which is the measure of the voidage or emptiness of the porous media.

Nomenclature			
		τ_r	particle relaxation time (s)
		d_p	particle diameter (µm)
DPM	Discrete Phase Model	Re	Reynolds number
IBM	Immersed Boundary Method	C_d	drag coefficient
DEM	Discrete Element Method	m_p	particle mass (kg)
MPM	Macroscopic Particle Model	$c_{p,p}$	particle heat capacity (J K^{-1})
UDF	User Defined Function	h	convective heat transfer (w/m^2K)
CAD	Computer Aided Design	A_p	surface area of the particle (m^2)
PR-DNS	Particle Resolved Direct Numerical Simulation	T_∞	local temperature of the fluid (K)
		ε_p	emissivity of the particle
FVM	Finite Volume Method	σ	stefan boltzmann constant
PPI	Pores Per Inch	θ_R	radiation temperature (K)
LBM	Lattice Boltzmann Method	α	thermal diffusivity (m^2/s)
		ν	kinematic viscosity (m^2/s)
S_m	source mass (kg)	µ	dynamic viscosity (Pa.s)
p	static pressure (Pa)	S_T	transverse pitch (mm)
$\vec{g}$	gravitational force (m/s^2)	d_f	ligament diameter (cm)
$\vec{F}$	external body forces (N)	d_p	pore diameter (cm)
I	unit tensor	ε	porosity
μ	molecular viscosity (m^2/s)	Nu	Nusselt number
J_j	diffusion flux (m^{-2} s^{-1})	k_f	fluid thermal conductivity ($Wm^{-1}K^{-1}$)
S_h	heat of chemical reaction (kj/mol)	V_f	fluid velocity (m/s)
Y_j	mass fraction of species	V_p	particle velocity (m/s)

Heat transfer devices are becoming smaller and consume more energy and the use of metal foams are seen as a suitable heat transfer device to dissipate heat for electronics cooling applications, namely integrated circuits such as graphics cards, CPUs, hard disk drives, among others. Additionally, these porous metal foams could be deployed in HVAC&R systems under specific conditions and even for exhaust gas recirculation systems (EGR). A myriad of numerical and experimental studies was conducted to better understand the thermal and fluid flow characteristics such as thermal conductivity, pressure drop, Nusselt Number and friction factor. According to these studies, metal foam structures have very good heat transfer characteristics as high thermal conductivity especially due to a large surface to volume ratio but they exhibit large pressure drop, and depending on the operating conditions, the pressure drop of metal foam heat exchangers are significantly higher than conventional plate-fin heat exchangers. For example, the Reynolds number has a significant effect on pressure drop (Leong and Jin 2006) and Zhao (2012) provided an analysis of the thermal transport mechanisms of open-cell foams. Their studies include convection, conduction and radiation. Schampheleire et al. (2013) studied the efficacy of metal foam heat exchangers for HVAC&R applications. It was found that metal foam heat exchangers perform better than conventional plate-fin heat exchangers under pure convective flow conditions whereas fin heat exchangers exhibit better performance at air velocities higher than 2 m/s. Mahdi et al. (2006) studied the deployment of aluminium foam heat exchangers for electronics cooling (CPU) applications and it was found that the thermal resistance is close to 70% lower compared to common fin heat exchangers. Wang et al. (2016) concluded that the maximum power generation of a thermoelectric generator (TEG) embedded with metal foams showed a 30 % increase as compared to a TEG without metal foam inserts. Nawaz et al. (2017) investigated the thermal hydraulic

performance of air-cooled metal foam heat exchangers under dry operating conditions. One of the main findings was that foams with a smaller pore size (*i.e.* corresponding to 40 PPI) have a higher heat transfer coefficient as compared to larger pore size metal foams (5 PPI). Seyf & Layeghi (2010) studied the heat transfer performance of a fin heat sink and compared the results with a fin heat sink embedded with metal foams. One of the main findings showed that an increase in Reynolds number and decrease in foam porosity resulted in a 400 % increase in the Nusselt number. Bai & Chung (2011) concluded that the heat transfer rate of a foam-filled tube is about two orders of magnitude higher as compared to an open unfilled tube. Metal foam heat exchangers can be used in various industrial applications. However, due to the large fluid resistance (*i.e.* pressure drop), metal foams are preferably deployed in certain engineering systems such as heating, ventilation, air-conditioning and refrigeration systems and electronics cooling (Schampheleire et al., 2013; Bayomy et al., 2016). For instance, at very high Reynolds number (inlet velocities), the pressure drop of metal foam heat exchangers is very high compared to traditional fin heat exchangers but metal foam heat exchangers was found to exhibit better thermal performance than fin heat exchanger when comparing the airside convective resistance only (Schampheleire et al., 2013). Interestingly, a hybrid metal foam - fin heat exchanger (*i.e.* finned-metal-foam heat exchanger) was found to outperform standalone plate-fin heat exchangers and metal foam heat exchangers (Krishnan et al., 2012). The operating conditions also play a key role in the performance of metal foam heat exchangers, for instance if was found that under impinging air jet cooling, the thermal performance of a hybrid metal foam finned heat exchanger is 1.5-2.8 times greater than standalone metal foam heat exchangers (Feng et al., 2014).

Clearly, metal foam heat exchangers are seen to exhibit superior thermal performance under specific conditions. However, it is noteworthy that the majority of these studies are based on two major assumptions. Firstly, all the metal foam heat exchanger studies assume single-phase fluid flow. This is not entirely correct because the vast majority of industrial applications such as power generation are based on multiphase solid-fluid flows, namely solid-gas and solid-liquid flows (Traore et al., 2015). Unfortunately, there are very limited studies that critically examine the complete fundamental aspects of multiphase solid-fluid flows and solid particulate fouling in metal foam heat exchangers. There are limited studies on multiphase solid-fluid flows through metal foam heat exchangers; however, these studies assume isothermal flows in which no heat transfer effects where considered (Kuruneru et al., 2016; Kuruneru et al., 2017a; Kuruneru et al., 2017b; Kuruneru et al., 2017c; Kuruneru et al., 2018). Secondly, the effects of solid particulate fouling coupled with heat transfer effects in porous media was not considered.

Fouling is a major problem in the industry. In particular, a major challenge in the peak operation of a heat exchanger, regardless of whether it's a plate-fin or metal foam heat exchanger, is the presence of impurities or solid foulants which results in a reduction of the heat exchanger efficiency and thermal performance. Particulate fouling is defined as an accumulation and deposition of unwanted material or dust inside a heat exchanger. In particular, this unwanted solid foulants or solid particles are present in the working fluids that pass through the heat exchanger. The presence of these particles on the heat exchanger's surface reduces the thermal efficiency and increases the pressure drop. This in turn could potentially lead to an increase in energy consumption, greenhouse gas emissions, intermittent shutdown of heat exchangers and maintenance costs. In addition, this could also lead to a large uncertainty in heat exchanger design. According to statistics the economic penalties incurred due to heat exchanger fouling in major industrialised countries is about US $ 4.4 million every year and it was found that the losses due to heat exchanger fouling are about 0.25% to 0.35% of the GPD (Gross Domestic Product) of industrialized nations (Pritchard 1988). For example, Steinhagen et al. (1993) estimated that heat exchanger fouling in New Zealand accounted for about 0.15% of the GNP (Gross National Product). A study showed that the energy and economic penalties for the US refineries due to fouling cost more than $4 million every year (Panchal and Huangfu 2000). Thackery (1980) estimated that fouling corresponds to about 15% of the maintenance costs of a process plant can be attributed to heat exchangers and boilers. It was found that utility fouling in China accounts for about $4.68 billion which represents 0.17% of GDP of China (Zhi-Ming, Zhong-Bin et al. 2007). Clearly, fouling is a multifaceted problem in the industry which infers the significance of the development of antifouling strategies.

A number of antifouling heat exchanger techniques and strategies were developed over the years but fouling continues to remain a complex and multifaceted problem and even if a heat exchanger is perfectly designed to maximize the thermal performance, fouling can mitigate the heat transfer performance (Müller-Steinhagen, Malayeri et al. 2011). There are various antifouling mitigation strategies available in the market, but a number of these antifouling techniques have many drawbacks such as high cost, toxic, and requirement of laborious work for installation and implementation of antifouling techniques, among others. The interested reader is referred to (Müller-Steinhagen et al. 2011) for an in-depth review of fouling mitigation strategies. Metal foam heat exchangers could potentially have a greater tendency to be subject to fouling due to the stochastic and irregular nature of these porous structures. Moreover, the cleaning process is quite difficult and even for this reason true potential of this porous metal foam heat exchangers is still indistinct. For example, the surfaces of a metal foam heat exchanger could be easily infected by particle deposition or particulate fouling, and the severity of fouling depends on a myriad of factors such as particle size, fluid density, fluid and particles

velocity, particles concentration and temperature, among others. In particular, even the stickiness, the repulsive forces, the attractive forces between particles, the wettability and the roughness of the surfaces in which deposition could occur are important parameters to check. However, a recent study has shown that oscillating pulsatile fluids play an important role in reducing or even nullifying particulate fouling in metal foam heat exchangers depending on the frequency of the pulsatile fluids (Kuruneru et al., 2018).

The objective of this research is to develop a numerical model to examine the transient evolution of a multiphase solid-fluid flows and to study the interaction between the solid particles and the fluid inside a simplified geometry of a metal foam heat exchanger. The authors' intent is to create a model that is approximate and easily compared with the applications in which metal foam heat exchangers are installed. In this study, different working fluids, particles and fluids inlet velocities, wall temperatures and particles densities are modelled. The maximum temperature of the solid foulants are analysed and discussed. ANSYS Fluent is used to numerically simulate non-isothermal solid-fluid flows in idealized metal foam structures. In addition, the Macroscopic Particle Model (MPM), which is an advanced add-on module available in ANSYS Fluent, is deployed in order to inject the particles into the porous media. This advanced add-on module is capable of predicting the behaviour of particles and to analyse the interactions between particle-fluid, particle-walls and particle-particle. Using the standard Discrete Phase model (DPM), the particles are treated as point particles (negligible volume) that do not interact with one another. As such, the use of MPM allows the end-user to capture solid-wall interactions and is also used when the grid is comparatively small compared to the size of the solid discrete particles. The MPM module allows the end-user to account for various effects such as particle-particle interactions and particle-wall collisions, the blockage of fluid, the evolution of the drag force and torque experienced by the particles, the friction dynamics, among others. To the best of the authors' knowledge this one is the first research based on solid-fluid flows through an idealized metal foam heat exchanger using the advanced Macroscopic Particle model in ANSYS Fluent.

A numerical investigation of multiphase solid-fluid flows through an X-ray μ-CT reconstructed metal foam structure is extremely computationally expensive. Obtaining such digitized metal foam scans via X-ray μ-CT is time-consuming, difficult and expensive. Secondly, multiphase solid-fluid flows through reconstructed metal foams both at macroscopic and pore-level is not examined in the literature. For this reason, many researchers propose the use of alternative metal foams in the form of Weaire-Phelan or Kelvin model which is a close representation to the real metal foam structure, especially to analyse the pressure drop and heat transfer mechanisms. For example, Chung et al. (2006) numerically analysed the pressure drop of an open-cell foam based on the Kelvin structure using hydrogen as a coolant and the authors compared their numerical results against experimental data published by Leong and Jin. The numerical results align well with the experimental results but the Kelvin model underestimates the pressure drop (Leong and Jin 2005). Boosma et al. developed a similar approach based on Weaire-Phelan structure and according to these authors the model can underestimate the pressure drop (Boomsma, Poulikakos et al. 2003). One possible reason is that the surface roughness of the model was not accounted for. Kuruneru et al. (2016) concluded that Weaire-Phelan models can be used for heat exchangers where low Reynolds number is prevalent such as HVAC&R systems and the Weaire-Phelan model can overestimate the pressure drop at high Reynolds number. Many researchers have used cylindrical arrays of circular struts which is a simple representation to the real metal foam geometry at the pore-level (Dukhan, 2005; Fuller, 2005; Ghosh, 2009; Hooman, 2012; Tamayol, 2011; Mahjoob & Vafai, 2008). The authors intention is to delve into the solid-fluid heat transfer characteristics at the pore-level as a first step prior to studying solid-fluid flows through the real metal foam structure at macroscopic level which is the subject for future research. As such, in this study, we use a 3D array of cylindrical cylinders similar to the geometries presented in previous studies Dukhan, 2005; Fuller, 2005; Ghosh, 2009; Hooman, 2012; Tamayol, 2011; Mahjoob & Vafai, 2008).

This study serves as a basis for future studies pertaining to particle deposition and particle aggregation in a metal foam heat exchanger. In fact nowadays in many technological processes high temperatures are prevalent and the knowledge of the maximum temperature of the solid particles in metal foam heat exchangers could be very important and beneficial when it comes to studying, for example, the adhesiveness between the solid foulants and the heat exchanger walls in addition to the cohesion between solid foulants. The temperature is in fact one of the most important properties that has a considerable effect on all the physical mechanisms of fouling in metal foam heat exchangers. As such, in this study, the maximum temperatures of the solid particles in the metal foam heat exchanger is analysed and compared based on different solid-gas thermo-physical properties, Reynolds number, and metal foam ligament temperature.
This document is organised as follows. In **Section 2**, the numerical methodology, namely the finite volume method and the advanced Macroscopic Particle Model (MPM) add-on model is discussed and is presented. Then details of the computational domain and the computational mesh are presented in **Sections 3** & **4** respectively. Afterwards, we discuss about the case studies which is presented in **Section 5**. The validation of the numerical model and the complete analysis and discussion of multiphase non-isothermal solid-fluid flows through porous media is discussed in **Section 6**. Finally, the conclusions and perspectives are covered in **Section 7**.

2. Numerical Model

2.1. Governing Equations:

In this research, the transient multiphase solid-fluid flow inside a porous media geometry is investigated at the pore-level and the governing equations are based on the Navier-Stokes equations (ANSYS Fluent 2011). A coupled finite volume method (FVM) and the macroscopic particle model (MPM) is developed and implemented in ANSYS Fluent with the overarching goal of analyzing the heat transfer between the working fluid, the solid particles and the metal foam ligaments. ANSYS Fluent solves conservation equations for mass, momentum and energy for the fluid phase.

$$\frac{\partial \rho}{\partial t} + \nabla \cdot (\rho \vec{v}) = S_m \tag{1}$$

where S_m is the mass added to the continuous phase from the dispersed second phase. The conservation of momentum in an inertial reference frame is given by:

$$\frac{\partial}{\partial x}(\rho \vec{v}) + \nabla \cdot (\rho \vec{v}\vec{v}) = -\nabla p + \nabla \cdot (\rho \bar{\bar{\tau}}) + \rho \vec{g} + \vec{F} \tag{2}$$

where p is the static pressure, $\rho \vec{g}$ is the gravitational body force and $\vec{F}$ is the external body forces that arise from interaction with the dispersed phase. The stress tensor $\bar{\bar{\tau}}$ is described by

$$\bar{\bar{\tau}} = \mu \left[(\nabla \vec{v} + \nabla \vec{v}^T) - \frac{2}{3} \nabla \cdot \vec{v} I \right] \tag{3}$$

where I is the unit tensor, μ is the molecular viscosity and the second term on the right hand side of the equation accounts for the volume dilation effect. The energy equation is given by:

$$\frac{\partial}{\partial t}\left(\rho(h - \frac{p}{\rho} + \frac{v^2}{2})\right) + \nabla \cdot \left(\vec{v}\left(\rho(h - \frac{p}{\rho} + \frac{v^2}{2}) + p\right)\right) = \nabla \cdot [k \nabla T - \sum_j (h_j \vec{J}_j) + \bar{\bar{\tau}} \cdot \vec{v}] + S_h \tag{4}$$

where J_j is the diffusion flux of species j and k is the thermal conductivity. The three terms inside the brackets on the right side of the energy equation represent, respectively, the energy transfer due to conduction, species diffusion, and viscous dissipation and the term S_h includes the heat of chemical reaction which is assumed negligible as combustion and chemical interactions and mass transfer is not considered in this study. The enthalpy h is defined as

$$h = \sum_j Y_j \left(\int_{T_{ref}}^{T} C_{p,j} dT \right) + \frac{p}{\rho} \tag{5}$$

where T_{ref} is 298.15 K, Y_j is the mass fraction of species j and the last term is zero if an ideal gas is considered.

In ANSYS Fluent, the trajectory of a solid discrete particle is evaluated by integrating the force balance on the particle that equates the inertia of the particle with the forces acting on it and this can be described by the following relation

$$\frac{d\vec{u}_p}{dt} = \frac{\vec{u} - \vec{u}_p}{\tau_r} + \frac{\vec{g}(\rho_p - \rho)}{\rho_p} + \vec{F} \tag{6}$$

where u and u_p are the fluid and particle velocity, ρ and ρ_p are the fluid and particle density, g is the force of gravity and the first term on the right side of the equation represent the drag force per unit particle mass and τ_r that is the particle relaxation time is defined by

$$\tau_r = \frac{\rho_p {d_p}^2}{18\mu} \frac{24}{C_d Re} \tag{7}$$

where d_p is the particle diameter, Re is the Reynolds Number and C_d is the drag coefficient. In the equation of the particle force balance the last term F includes additional forces as the force due to the pressure gradient in the fluid and the force required to accelerate the fluid around surrounding the particle which is called the virtual mass force. The heat balance

used in ANSYS Fluent to relate the particle temperature to T_p to the convective heat transfer and the emission or absorption of radiation on the surface of the particle is:

$$m_p c_{p,p} \frac{dT_p}{dt} = hA_p\left(T_\infty - T_p\right) + \varepsilon_p A_p \sigma\left({\theta_R}^4 - {T_P}^4\right) \tag{8}$$

where m_p and $c_{p,p}$ are the mass and the heat capacity of the particle, h is the convective heat transfer, A_p is the surface area of the particle, T_∞ is the local temperature of the fluid, ε_p is the emissivity of the particle, σ is the Stefan Boltzmann constant (5.67×10^{-8} W/m^{2}K^4) and θ_R is the radiation temperature. In this study, radiation is neglected as the temperatures considered herein are below 700 K.

2.2. Macroscopic Particle Model

In ANSYS Fluent, the traditional Discrete Phase Model (DPM) is applicable only with particles whose sizes are considerably smaller than the size of the mesh cell elements. In particular, the particles in the DPM model are treated as point masses and this model is used when the total particle volume is insignificant compared to the flow domain volume, and the particle-flow and particle-particle interactions are evaluated in terms of impulse, mass transfer and heat. However, in some models it is very important to consider the total particle volume because it can have a considerable effect on the fluid flow behaviour. For these specific cases, the Macroscopic Particle model (MPM), which is an advanced add-on module in ANSYS Fluent, permits engineers to predict the behaviour of particles and their interaction with the fluid flow, heat exchanger walls, and with other solid particles. The MPM is commonly deployed in numerical simulations in the even the solid particle size is significantly greater than the mesh cell size. It is noteworthy that the MPM is based on the user defined function (UDF) in ANSYS Fluent. The UDF is written in a programming language called C. The UDF can be loaded with ANSYS FLUENT to enhance and improve its standard features, in this case, alongside the DPM module. In the MPM model, each discrete particle that touches several mesh elements cannot be neglected during the simulation and this solid particle is represented by a sphere with six degrees of freedom to describe the particle rotation and translation as the particles are injected through the inlet plane and also as it traverses with the flow throughout the simulation. It is assumed that each particle touches one computational cell if one or more nodes of the cell are located inside the particle volume and each particle transport equation is solved in a Lagrangian reference frame. As we discussed earlier, the MPM model provides a special treatment for the flow blockage and momentum and energy exchange, drag and torque on particles, particle-particle and particle-wall collision, attraction forces and friction dynamics and particle deposition. The momentum transfer works as follows: a volume-fraction weighted velocity between the flow velocity in the cell at the last time step and particle velocity is assigned to the fluid mesh elements occupied by the particle and for this reason the flow velocity of these elements is affected by the particle velocity. All the collisions between particle-particle and particle-walls are assumed to be quasi-instantaneous and the contact is considered occurring at a single point because ANSYS Fluent follows the billiard ball model to account all these collisions. By using this algorithm, it is possible to consider the impulse forces and momentum experienced by the particles during the collision and even the energy dissipation.

Regarding the implementation of the particle deposition phenomenon, it is based on the critical impact velocity algorithm and if the particle velocity is larger than the critical impact velocity specified by the end-user, the particle will rebound from the wall after impact. However, if the particle velocity is smaller than the critical impact velocity then the particle will stop on the wall and the software will assign to it zero velocity and acceleration. The MPM is not a general-purpose model, and it has some limitations that are important to take into account in order to get accurate results. These limitations have been taken into account prior to running any numerical simulations in this study. Also, it is noted that the mass transfer and radiation cannot be modelled and simulations of densely-packed particles are not supported because only one collision event is managed for every particle time step and the sub-iterations of MPM particle tracks within one time step are not supported. Therefore, the Macroscopic Particle Model is not compatible with mesh interfaces or moving and deforming meshes. It is even shown that the model can give accurate results for the cases in which a study is based on laminar flow and where the ratio between the particle density and the particle fluid is close to unity. For other values of Reynolds number and density ratio, the prediction of the coefficient of drag may not be accurate and for these cases the MPM model may be used when drag is not important.

2.3. Solution Control:

The timestep for the fluid phase is set to 0.001 s and the particle sub-timesteps is set to 10. Five particles are injected after two timesteps in the fluid domain using the point injection in the MPM setup. The initial position of a particle is close to the velocity inlet plane located at the top of the geometry and the particle initial velocity and the fluid initial velocity is the identical. The simulation is executed until the last particle has exited the domain through the outlet plane. The residuals are set to 1×10^{-5} for continuity and velocity and to 1×10^{-6} for the energy. The particle-wall deposition

is enabled and the maximum normal and tangential velocity for the particle deposition are both set to 0.01 m/s. The number of collision resolution steps is set to 10. The under-relaxation factors used by the pressure-based solver are set to 0.3 for pressure, 0.7 for momentum and 1 for density, body forces and energy. For the fluid flow a "SIMPLE" algorithm is used to achieve a stable pressure and velocity coupling. For the spatial discretization a "Second Order Upwind" scheme is deployed for energy and momentum, a "Least Squared Cell Based" for the gradient and a "PRESTO!" discretization scheme is used for the pressure according to the use of Macroscopic Particle Model. These settings are widely used (Saha et a. 2011, Cui et al. 2015). For the transient formulation a "First Order Implicit" is used as solution formulation.

2.4. Model Assumptions:

The following assumptions are enforced in the numerical model:

1. The working fluid considered in this study, air and water, are assumed to be incompressible.
2. The solid particles are smooth and rigid.
3. Deformation of solid particles are assumed to be negligible.
4. Radiation effects are neglected as temperatures considered in this study are below 700K.

3. Geometry

The numerical model is developed and implemented to analyse solid-fluid multiphase laminar flows in addition to tracking the particles injected in the fluid domain with the goal of gaining new knowledge of the heat transfer between the particles, the working fluid, and the surfaces of the metal foam heat exchanger. In this study, the metal foam structure comprises a cubical array of cylindrical struts. The geometry is created using a computer aided design (CAD) program called SolidWorks and then the geometry is imported to ANSYS Designer Modeler. The dimensions of the geometry are 4 mm (length) × 4 mm (height) × 1 mm (thickness). The thickness of the geometry is designated because 3D simulations are a prerequisite for the Macroscopic Particle Model in ANSYS Fluent. Three rows each comprising three cylindrical circular obstructions is modelled and the nine cylinders have a diameter of 0.26 mm and they represent the metal foam ligaments. The vertical and the horizontal distances between the cylinders are 0.65 mm and the vertical and horizontal distances between the lateral cylinders and the symmetry walls are both 1.35 mm. The front surface has an area of 15.52 mm^2, the volume of the geometry is 15.52 mm^3 and a front view of the geometry considered in this paper is shown in **Fig. 1**.

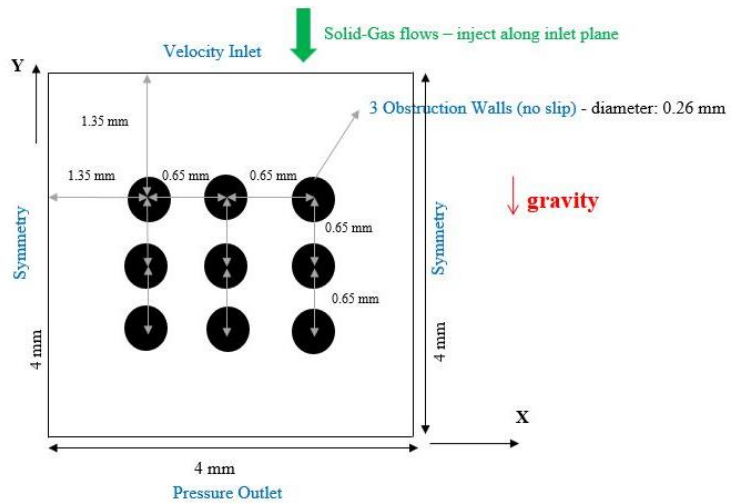

Fig. 1: Metal foam heat exchanger geometry.

The porosity of a metal foam can be evaluated by:

$$\varepsilon = 1 - \frac{3\pi}{4}\left(\frac{d_f}{d_p}\right)^2 \tag{9}$$

In **Equation (9)**, d_f is the ligament diameter and d_p is the pore diameter, according to the geometry shown in **Fig. 1** where d_f and d_p are, respectively, 0.26 mm and 0.65 mm, and a foam porosity ε of 62.3% is registered. In this study, we consider low-porosity foams because the majority of metal foam studies in the existing literature are based on high-porosity foams (*i.e.* ≥ 90%). However, Dukhan (2006) enunciated that these very high porosity foams may not be suitable for specific thermal applications and these foams have minuscule gain in heat transfer performance and these very light (porous) structures are structurally weak and may not be suitable for specific thermal applications. As such,

in this study, a low-porosity foam (≤ 90%) is considered. The other important parameter of metal foams is the *PPI* which represents the number of pores per linear inch (1 inch = 2.54 cm) and it can be approximated by the following **Equation (10)**:

$$d_f = \left(0.431 - 0.0049\text{PPI} + \frac{2.43}{\text{PPI}^2}\right) \tag{10}$$

According to **Equation (10)**, in this study, the number of pores per inch (*PPI*) is 35.

The decision to create just a small portion with only nine cylinders is due to the symmetrical nature of the problem and also due to the fact that the simulation of a multiphase solid-fluid flow with the use of the Macroscopic Particle Model (MPM) is very computationally demanding. As discussed earlier in the introduction, it is possible to use the MPM model to numerically simulate solid-fluid flows through reconstructed metal foams obtained via X-ray microtomography but this technique is very computationally demanding, expensive and time-consuming. As such, it is the intention of the authors to simulate a small portion of metal foam using a simplified geometry comprising ordered cylindrical arrays while retaining the macroscopic properties and characteristics of a real metal foam such as porosity and fibre thickness. Moreover, the authors' intention is to conduct a pore-level analysis of multiphase solid-fluid flows as a first step prior to assessing multiphase solid-fluid flows through a real metal foam structure.

With the use of this geometry it is assumed that the foam porosity is constant and there are no important variations in the macroscopic properties of the foam (*i.e.* non-variable porosity media). The idea is to use this type of geometry to model the real metal foam which was also used by many authors, for example, Dukhan et al. (2005) provided a heat transfer analysis based on a bank of cylinders. Ghosh (2008) published an in depth analysis of the heat transfer mechanism using a bundle of independent and slender tubes to simulate the metal foam. Tamayol presented an analytical analysis of the viscous permeability of fibrous porous media using a model of a simple cell (Tamayol and Bahrami 2008). Bhattacharya and Mahajan (2002) presented a numerical analysis of the pressure drop in metal foam using a 3D array of cylinders. Buonomo et al. (2016) used a similar geometry to numerically analyse a single phase flow (air) in an aluminium metal foam heat exchanger. Wang et al. (2017) numerically investigated fouling in metal foam using a 3D geometry with two cylinders. However, in this study, the target is to investigate the heat transfer between the particles, the fluid, and the surfaces of the metal foam. As such, the geometry shown in **Figure 1** is chosen as the computational domain. Additionally, the authors' intention is to provide a numerical analysis of multiphase flows based on this simplified geometry. This could serve as a steppingstone to study multiphase flows in real and more complex open-cell metal foam structures. As shown in **Figure 1**, six different inlet velocities are assigned at the top plane, and zero pressure outlet is assigned at the bottom plane. A no-slip boundary condition is assigned to the nine cylindrical ligaments of the metal foam. Symmetry boundary conditions are applied to the right and left walls and it assumed that these planes are permeable to the solid particles.

4. Computational Mesh

The use of the Macroscopic Particle Model requires that each particle injected in the domain occupies more cells and the mesh element size must be smaller than the particle diameter size. The smallest particle size considered in this study is set to 100 micrometers in order to comply with the MPM protocols such as the mesh cell size. To select a good mesh, a grid independent test is performed using different meshes. This grid convergence study is conducted to analyse the quality of the mesh and how the mesh density can influence the numerical results, namely pressure drop. In addition, this grid convergence study is used to find a good equilibrium of the results with the minimum number of nodes and elements in order to decrease the computational time. The mesh is refined by changing the 'sizing option' in ANSYS mesh, in addition, other parameters such as the minimum, maximum and average element quality and skewness are checked for each mesh and compared. For the mesh, linear hexahedral elements with 8 nodes each (HEX8) is used. The pressure drop of various mesh qualities are analysed using the volume rendering options available in ANSYS CFD-Post. The number of nodes of the four different meshes are: 264836, 398550, 496352 and 1057964. According to **Table 1** and **Table 2**, the mesh with 496352 nodes (Grid 3) has a pressure drop value very similar to the finer mesh (Grid 4). As such, grid 3 is used in the remaining studies. In addition, the mesh sensitivity analysis is shown in **Fig. 2**.

Table 1 Pressure drop based on various grids.

Grid	Number of nodes	ΔP (Pa)
1	264386	2.61E-02
2	398550	2.82E-02
3	496352	2.92E-02
4	1057964	2.91E-02

Table 2 Calculation of absolute, relative and percentage errors.

Mesh B – Mesh A	Absolute error	Relative error	% error
Mesh 2 – Mesh 1	0.002138	0.07572	7.572
Mesh 3 – Mesh 2	0.000931	0.03190	3.190
Mesh 4 – Mesh 3	0.00011	0.00380	0.380

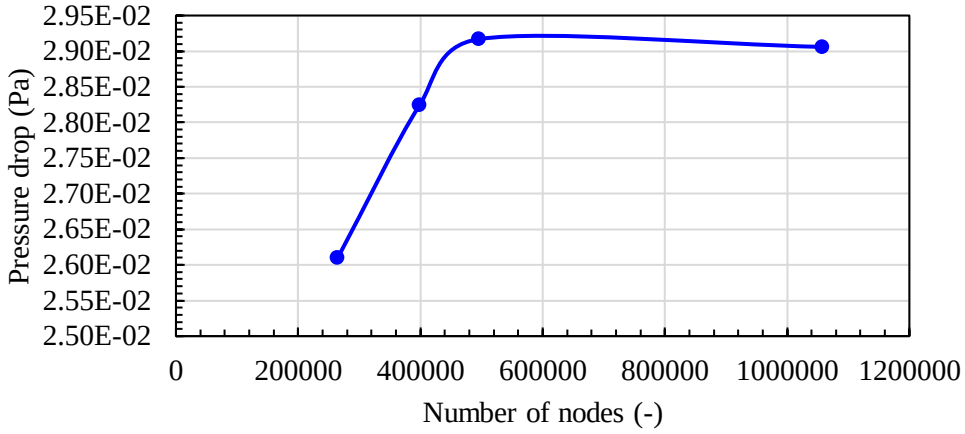

Fig. 2: Mesh sensitivity analysis.

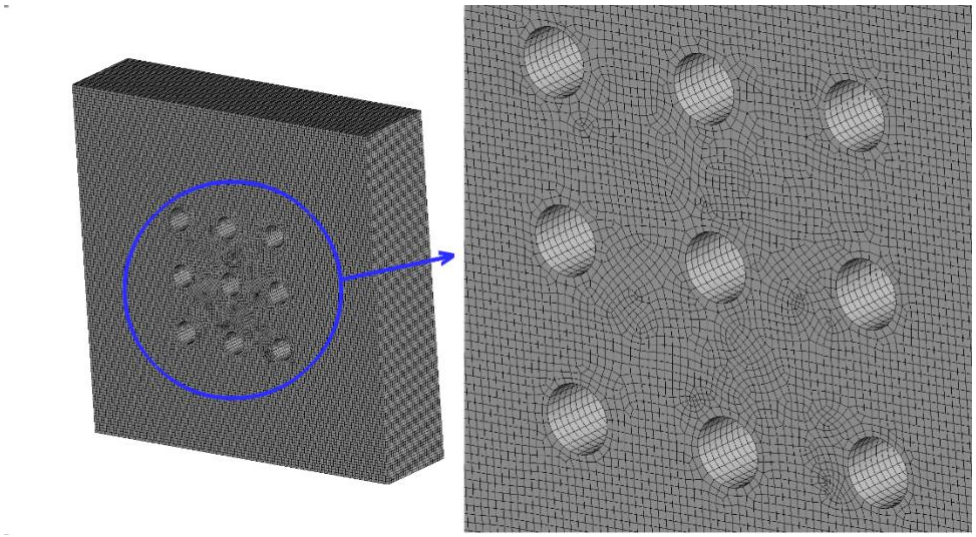

Fig. 3: Computational mesh.

5. Case studies

A total of 168 different studies are investigated as shown in **Table 8** in the appendix of this manuscript. Air and water are used as the primary working fluids and their properties are shown in **Table 3**.

Table 3 Properties of the working fluids.

Fluid	ρ_f [kg/m^3]	C_p [J/kg·k]	k_f [W/m·k]	M_f [kg/kmol]	μ_f [Pa·s]
Air	1.23	1006.43	0.0242	28.97	1.79E-05
Water	998.20	4182	0.6	18.01	1.00E-03

The Prandtl Number is calculated for both fluids using the following **Equation (11)**:

$$\mathrm{Pr} = \frac{\nu}{\alpha} = \frac{\mu C_p}{k} \tag{11}$$

where μ, C_p and k are, respectively, the dynamic viscosity, specific heat capacity and thermal conductivity of the fluid. This dimensionless quantity depends only on the fluid and it is defined as the ratio between the kinematic viscosity (ν) and the thermal diffusivity (α). According to this formula, the Prandtl number is 0.74 for air and 6.99 for water. In this study, three different particle diameters are investigated: 500, 250 and 100 micrometres (Hosseini et al., 2017) and the particle densities and thermal properties are shown in **Table 4**.

Table 4 Properties of discrete solid particles.

d_p [μm]	ρ_p [kg/m^3]	C_p [J/kg·k]	k_p [W/m·k]
500	1500	1680	0.33
250	1500	1680	0.33
100	1500	1680	0.33
500	8960	381	386.60

In all the numerical simulations, the particle initial temperature is set to 300 K and the inlet working fluid temperature is set to 300 K as well. Regarding the temperature of the metal foam ligaments, T_{cw}, four different values are studied in this project: 315 K, 330 K, 350 K and 400 K. In addition, six different inlet particle and fluid inlet velocities, U_∞, are analysed with a minimal velocity of 0 m/s followed by 0.01 m/s, 0.05 m/s, 0.1 m/s, 0.15 m/s and 0.25 m/s. These velocities are prevalent in specific HVAC&R applications (John, 2011; Schampheleire et al., 2013). A total of five solid particles are injected along the inlet plane at the start of the simulation. The solid particle (foulant) initialization velocity $U_{f\text{-}i}$ is the same as the fluid inlet velocities. The solid particle (foulant) densities correspond to anthracite (1500 kg/m^3) and copper (8960 kg/m^3). The coefficient of friction is set to 0.5 for both the particle-particle and particle-wall (metal foam ligaments) collisions. The coefficient of restitution is set to 0.5 and this assumption is based on 100% sticking probability for many heat transfer equipment as HVAC&R and was used by various authors in the past (Afkhami et al., 2015). This range of inlet particle and fluid velocity results in laminar flow as only laminar flows are considered in this study. The Reynolds number is calculated as:

$$Re = \frac{\rho V L}{\mu} \tag{12}$$

where V is the inlet fluid velocity, ρ and μ are, respectively, the working fluid density and dynamic viscosity, and L is the characteristic linear dimension in SI units. However, for the geometry considered in this paper, **Equation (13)** provides a more accurate representation of the fluid flow through this type of geometry (Bergman, Lavine et al. 2011):

$$Re = \frac{\rho V_{max} D}{\mu} \tag{13}$$

In fact this configuration which is similar to a bank of tubes aligned in the direction of the fluid velocity V, is characterized by the tube diameter D of 0.26 mm (metal foam ligaments diameter) and by the transverse pitch S_T and longitudinal pitch S_L measured between the middle of the ligaments which are both equal to 0.65 mm. So in this case, the Reynolds number is based on the maximum fluid velocity V_{max} occurring within the tube bank and for the aligned configuration of tubes it is recorded at the transverse plane between two ligaments; V_{max} can be obtained by the following equation by accounting for the fluid velocity inlet V:

$$V_{max} = \frac{S_T}{(S_T - D)} V \tag{14}$$

The full details of the case studies are presented in **Table 8** in the Appendix section.

6. Results

6.1. Numerical model validation

The numerical model validation is a very important part of this research and it is performed to demonstrate the accuracy of the Macroscopic Particle Model. For this step the typical case of the bouncing motion of a Teflon particle immersed in a glass box with a quiescent fluid is used to validate the numerical model and the results are compared with experimental values and with numerical values obtained by other authors. The box dimensions are 120 mm × 120 mm × 120 mm and at the beginning of the simulation the particle is injected using MPM at a height of 0.06 m where the fluid is quiescent. The solid Teflon particle has a diameter of 0.006 m and a density of 2150 kg/m^3 and the fluid present in the box is air with a kinematic viscosity of 1.6×10^{-5} m^2/s and a density of 1.225 kg/m^3. The restitution and friction coefficients of the particle-wall interactions are set to 0.8 and 0 respectively. After the particle is injected into the box

along the inlet plane, at 0s, the particle velocity increases as it traverses towards the bottom of the wall under the action of the gravity evidently settling down and reaching 0m/s at the bottom wall at around 0.11s. Once the particle impacts the bottom wall at 0.11s, as shown by the lowest point in **Fig.4a**, the particle bounces off the bottom wall, and then the particle velocity increases, and finally the particle attains a maximum height at around 0.20s before reaching 0 m/s. The lowest point of the graph shown in **Fig.4a** means that the particle has just reached the bottom of the wall and at that instance the particle velocity is 0 m/s as shown in **Fig.4b**. The data pertaining to this validation is shown in **Table 5**.

Table 5 Validation model.

Box Dimension	
Height [m]	0.12
Length [m]	0.12
Thickness [m]	0.12
Teflon Particle	
Initial Height [m]	0.6
Diameter Size [m]	0.006
Density [m]	2150
Fluid (Air)	
Kinematic Viscosity [m^2/s]	1.60×10^{-5}
Density [kg/m^3]	1.23
Molecular Weight [kg/kmol]	28.97

The particle position and the particle vertical linear velocity is observed at different time points and the values are analysed and compared against the experimental results. These numerical results are compared against the experimental data of Gondret et al. (2002) and particle resolved direct numerical simulation (PR-DNS) numerical results of Luo et al. (2016). In fact, the same case was simulated by Gondret et al. (2002) for testing the accuracy of the normal component of normal force and by Luo to validate his numerical model. The transient evolution of the particle's height and of the particle's velocity based on the different studies is shown in **Fig. 4**.

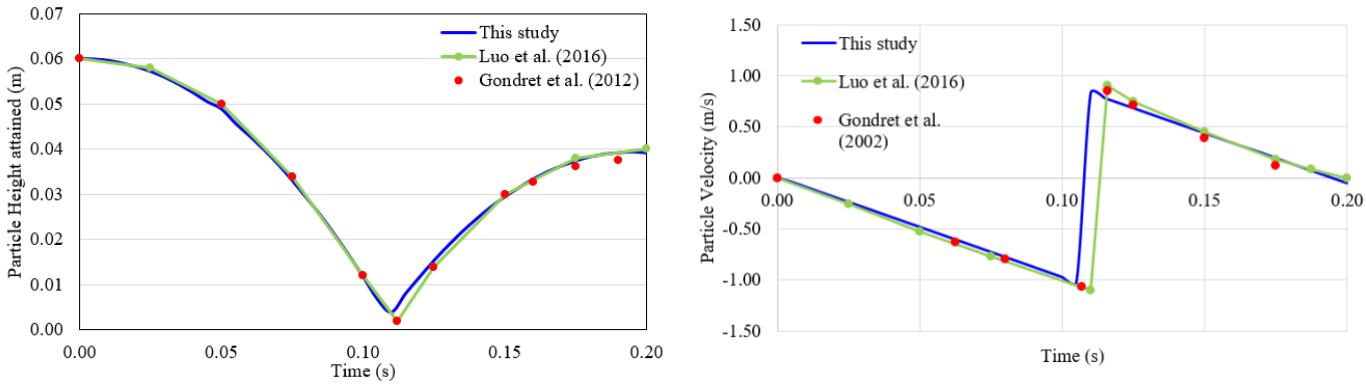

(a) (b)

Fig. 4: comparison with experimental data by Gondret et al. (2002) and numerical data by Luo et al. (2016) (a) particle position vs. time (b) particle velocity vs. time.

These charts show that the results obtained using Macroscopic Particle Model are in a very good agreement with the findings by Gondret et al. (2002) and Luo et al. (2016) thereby lending credence to the developed numerical MPM model. The small differences between this study and experimental data are considered completely acceptable and one of the cause of this discrepancy could be the fact that in this numerical model the bottom wall is completely smooth unlike the real one used for the experiment which has a roughness value even if very small. This small discrepancy is visible on the graphs when the particle is near the bottom wall and it is also reported by Zhang et al. (2014) in their numerical analysis using LBM-IBM-DEM (lattice Boltzmann method-immersed boundary method-discrete element method) to analyse the sedimentation of 2D circular particles in incompressible Newtonian flows. A similar observation was found by Feng and Michaelides pertaining to the deployment of a direct numerical method called Proteus to simulate and analyse the particulate flow (Zhang, Tan et al. 2014), (Feng and Michaelides 2005).

After validating the particle velocity and trajectory, the next step is to validate the heat transfer between the particle and the working fluid. This particular validation is performed because all the studies in this research delve into the maximum temperature of the particles in metal foam heat exchangers. In particular, the Nusselt number of a heated particle is numerically evaluated in ANSYS Fluent and compared with the Ranz-Marshall equation (Ranz 1952):

$$Nu = \frac{hD_p}{k_f} = 2 + 0.6\sqrt[2]{Re_p}\ \sqrt[3]{Pr} \tag{15}$$

where h is the heat transfer coefficient in W/(m²K), D_p is the particle diameter in m, k_f is the fluid thermal conductivity in W/(m·K), Pr is the Prandtl number of the fluid and Re_p is the particle Reynolds number calculated by:

$$Re_p = \frac{\rho_f D_p (V_f - V_p)}{\mu_f} \tag{16}$$

where ρ_f and μ_f are, respectively, the fluid density and the fluid dynamic, and V_f and V_p are the fluid and particle velocity. The properties of this heat transfer validation are shown in **Table 6**.

Table 6 Heat transfer validation model data and properties.

Fluid Property	
Density [kg/m^3]	998.20
Dynamic viscosity [Pa·s]	0.001003
Thermal conductivity [W/m·k]	0.60
Fluid specific heat capacity [J/kg·k]	4182
Solid Particle Property	
Diameter size [m]	0.0005
Density [kg/m^3]	8960

We compare the numerical and analytical values of the Nusselt numbers of two solid discrete particles at different velocities, as shown in **Table 7**. The numerical values of the Nusselt number is obtained from ANSYS Fluent whereas the analytical Nusselt number is obtained from the Ranz-Marshall correlation (*c.f.* eq. 15). Clearly, the numerical results closely align with the analytical equations of Ranz-Marshall and a very small discrepancy is observed between the numerical and analytical Nusselt number thereby demonstrating the accuracy of the developed numerical model in solving heat exchange problems.

Table 7 Comparison of the results obtained by ANSYS Fluent (numerical) with Ranz-Marshall equation.

	Particle	**V_f [m/s]**	**V_p [m/s]**	**Re**	**Pr**	**Nu**
Ranz-Marshall	A	0	0	0	6.99	2.00
Numerical result	A	0	0	0	6.99	2.01
Ranz-Marshall	B	0.26	0.215	22.40	6.99	7.43
Numerical result	B	0.26	0.215	22.51	6.99	7.44

6.2. Solid-fluid heat transfer characteristics

The transient multiphase solid-fluid flow namely, solid-liquid and solid-gas flows, through a porous geometry is studied. The momentum and energy transfer between the solid discrete particles and the metal foam circular cylindrical ligaments and the working fluids are considered in this research. The foulants are injected in the fluid domain with an initial velocity and, as time elapses, they traverse through the porous geometry towards the outlet. As we discussed in the introduction of this paper, the maximum temperature reached by the particles passing close to the heated ligaments of the metal foam is analysed, because this parameter can be very important for more complex researches pertaining to the cohesiveness between the particles or the particles adhesion with the metal foam ligaments and particle aggregation. The cases shown in **Fig. 5**, correspond to particles with density of 1500 kg/m^3 and air is the working fluid (*i.e.* solid-gas flows). The maximum temperature of the particles is plotted against the six different inlet velocities simulated in this research and these results are compared with the four different metal foam ligaments temperatures simulated. It is shown that with the increase of the particle and fluid initial velocity the temperature decreases, this is due to the fact that with the increase of the velocity the particle residence time (*i.e.* the amount of time a particle is immersed inside the porous structure) inside the geometry decreases and for this reason the heat exchange between the solid particles and the metal foam ligaments is gradually lower. It is even noticed that for the same reason the differences between the four cylinders temperatures are gradually decreasing with the increase of the velocity.

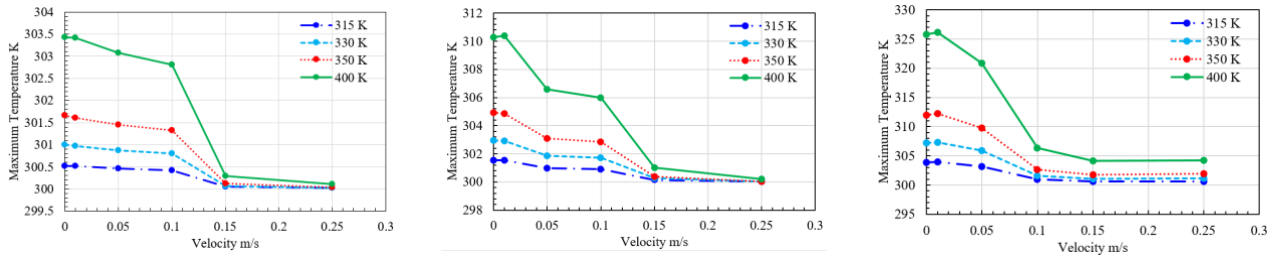

(a) (b) (c)

Fig. 5: Particle inlet velocity vs particle maximum temperature based on four different cylindrical ligament wall temperatures. Working fluid = air. ρ_p = 1500 kg/m^3. (a) d_p= 500 µm (b) d_p= 250 µm (c) d_p= 100 µm.

The cases are repeated albeit the use of water (i.e. solid-liquid flows) as the working fluid is considered, as shown in **Fig. 6**. The trend on these graphs are similar but the temperatures reached by the particles in the water flow are higher as compared to the previous cases with air (*c.f.* **Fig. 5**), and this is obviously due to the solid-fluid density ratios ρ_p/ρ_f. This ratio affects the amount of time a solid particle has spent inside the porous geometry (*i.e.* foulant residence time). The cases with air have a higher solid-fluid density ratio than the cases based on water, and as such, the particles immersed in air sediment towards the outlet faster than the particles immersed in water thereby not giving enough time for the particles in air to exchange heat with the heated cylindrical wall as compared to the case with particles immersed in water. In addition, the different properties of the fluids, in particular the different thermal conductivity of the fluids contribute to the differences in maximum foulant temperatures. It is noteworthy that minimum discrepancy in the maximum temperature profiles of foulants is observed at inlet velocities U_∞ commencing at 0.15 m/s for air and 0.10 m/s for water.

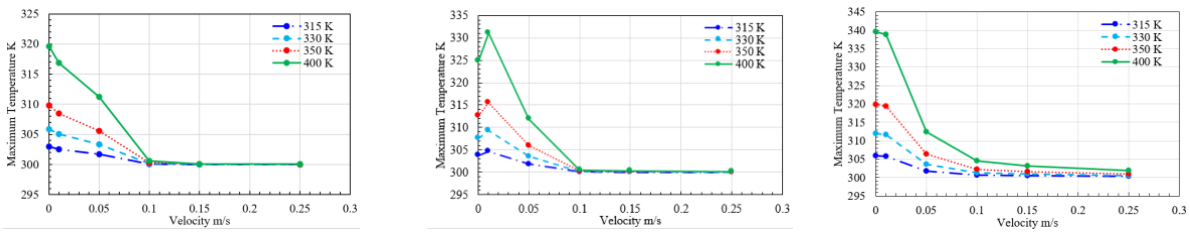

(a) (b) (c)

Fig. 6: Particle inlet velocity vs particle maximum temperature based on four different cylindrical ligament wall temperatures. Working fluid = water. ρ_p = 1500 kg/m^3. (a) d_p= 500 µm (b) d_p= 250 µm (c) d_p= 100 µm.

The same parameters are checked with air and with water for the copper particles (8960 kg/m^3) with diameter size of 500 µm and shown in **Fig. 7**. Interestingly, according to **Fig. 6** and **Fig. 7**, although the copper particle is more conductive than the anthracite particle (*c.f.* **Table 4**), the maximum temperature of the copper particle is very similar to the maximum temperature of the anthracite particle, this is because the ρ_p/ρ_f density ratio for copper is significantly higher than anthracite particle which means that the copper particles rapidly sediment towards the outlet plane and the highly conductive copper particle spends less time immersed in the domain (*i.e.* lower residence time). As such, due to the lower residence time of the copper, the copper has less time to exchange heat with the heated cylindrical ligament wall. The discrepancy between the maximum temperature of the foulants decreases with increasing inlet velocity and it becomes negligible at U_∞ = 0.25 m/s as at higher inlet velocities, the particles, together with the action of gravity, rapidly sediment towards the outlet thereby not enough time is realized for the particles to exchange heat with the heat cylindrical ligaments and the fluid surrounding these ligaments.

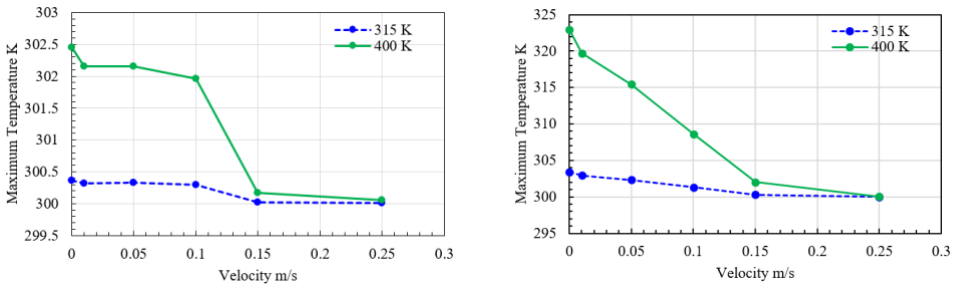

(a) (b)

Fig. 7: Maximum particle temperature based on various inlet velocities at two cylindrical wall temperatures at 315 K and 400 K. Working fluids (a) Air (b) Water. d_p = 500 µm, ρ_p = 8960 kg/m^3.

In **Fig. 8** and **Fig. 9**, the maximum temperature of the particles vs the metal foam ligaments temperature for the particle with 1500 kg/m^3 density and the two working fluids is shown. The results are compared with the different inlet velocities, and it is clear that increasing the metal foam temperature results in a gradual increase of the particle temperature. According to **Fig. 9**, the maximum temperature of the particles corresponding to inlet velocities of 0.10 m/s, 0.15 m/s, and 0.25 m/s are sensibly identical whereas a notable difference is observed at lower inlet velocities corresponding to 0 m/s, 0.01 m/s, and 0.05 m/s. At higher inlet velocities, the particles are unable to overcome fluid hydrodynamic shear as such the particles are quickly driven away from the geometry towards the outlet, and as such these particles do not have ample time to exchange heat with the heated cylindrical ligament wall. A linear trend is observed in all cases as shown in **Fig. 8** and **Fig. 9**.

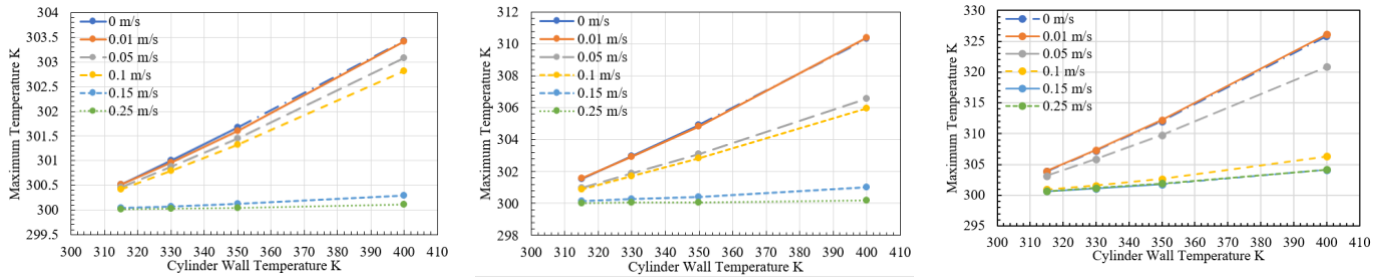

(a) (b) (c)

Fig. 8: Maximum solid particle temperatures based on various cylindrical ligament wall temperatures and inlet velocities. Working fluid = Air. ρ_p = 1550 kg/m^3. (a) d_p = 500 µm (b) d_p = 250 µm (c) d_p = 100 µm.

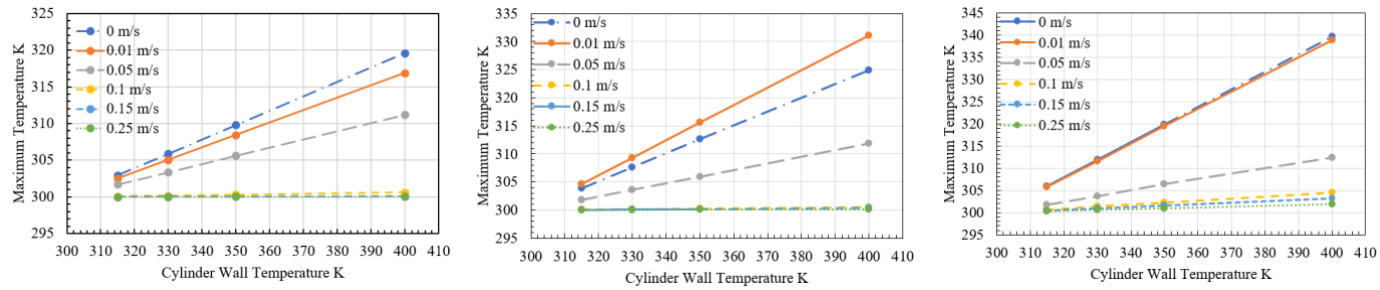

(a) (b) (c)

Fig. 9: Maximum solid particle temperatures based on various cylindrical ligament wall temperatures and inlet velocities. Working fluid = Water. ρ_p = 1550 kg/m^3. (a) d_p = 500 µm (b) d_p = 250 µm (c) d_p =100 µm.

The maximum temperature of copper particles (8960 kg/m^3) with diameter size of 500 µm is assessed and shown in **Fig. 10**. The maximum temperature of the copper particles increase with increasing cylindrical ligament wall temperature. This effect becomes less profound at lower inlet velocities regardless of the working fluid. This is because at higher inlet velocities, the particles are rapidly accelerated towards outlet plane thereby ample time is not realized for heat exchange between the solid foulants and heat cylindrical walls. The copper particles' maximum temperature, regardless of the working fluid, is very similar to the maximum temperature of the anthracites shown in **Fig. 8a** and **Fig. 9a** even though the copper foulant is more conductive than anthracite particles. This is because the heavier copper particles rapidly sediment away from the domain through the outlet plane and insufficient time is realized for heat exchange between these copper particles and the heated cylindrical wall.

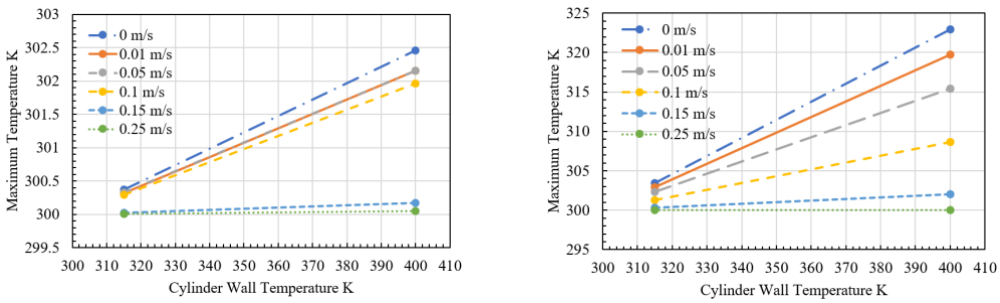

(a) (b)

Fig. 10: Maximum temperature of copper particles (d_p = 500 µm, ρ_p = 8960 kg/m^3) based on various cylindrical wall temperatures and inlet velocities. Working fluid (a) Air (b) Water.

For the sake of brevity, a comparative analysis of the maximum solid particle temperature based on various inlet velocities and metal foam circular cylindrical ligament temperature is shown in **Fig. 11** and **Fig. 12**. In these graphs, it is shown that for all the different inlet velocities, the highest temperatures are reached by the smallest particles.

Interestingly, for cases where the working fluid is air, the maximum temperature of the 100 µm particles are significantly higher than the 250 µm and 500 µm particles, whereas when the working fluid is water, the maximum temperature discrepancy is very similar regardless of the particle diameter. However, regardless of the working fluid, the 100 µm particles exhibit the highest maximum temperature. The maximum temperature of all foulants immersed in water or solid-liquid flows (*c.f.* **Fig. 12**) is higher than the maximum temperature of foulants immersed in air or solid-gas flows (*c.f.* **Fig. 11**), this is because the ρ_p/ρ_f density ratio in the case of water is lower than the case with air and the foulants immersed in water do not sediment as rapidly as compared to foulants immersed in air; as such, the foulants immersed in fluid have more time to exchange thermal energy with the heated cylindrical ligament thereby explaining the higher maximum particle temperature for solid-liquid flows shown in **Fig.12** unlike solid-gas flows shown in **Fig. 11**. Moreover, the maximum temperature of the particles remains sensibly invariant when the inlet velocity of the water is 0.1 m/s or greater (*c.f.* **Fig. 12**); whereas, the maximum temperature of the particles remains invariant with inlet velocity commencing 0.15 m/s when air as the working fluid is considered. A larger discrepancy between maximum foulant temperatures is realized at 0 m/s when the fluid is quiescent (U_∞ = 0 m/s). Higher inlet velocities infer lower maximum particle temperatures this is largely attributed to the fact the at higher inlet velocities, the fluid dissipates the heat around the heated circular cylindrical ligaments, in addition, the high inlet velocity has a greater probability to remove the particle away from the domain through the outlet plane.

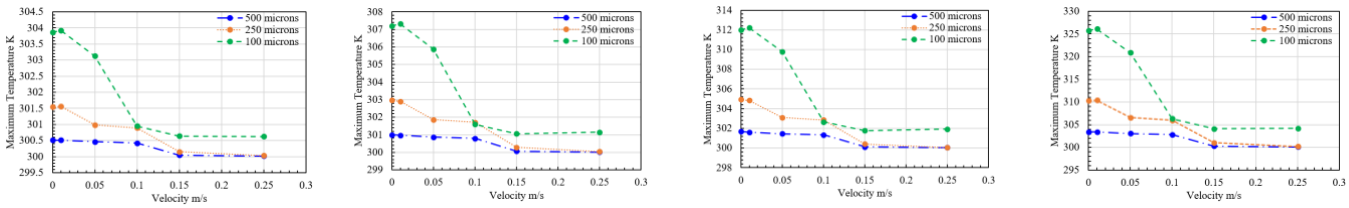

(a) (b) (c) (d)

Fig. 11: Maximum temperature of 100 µm, 250 µm, 500 µm solid particles based on various inlet velocities. ρ_p = 1500 kg/m^3. Working fluid = Air. Cylindrical ligament wall temperature T_{cw} = (a) 315 K (b) 330 K (c) 350 K (d) 400 K.

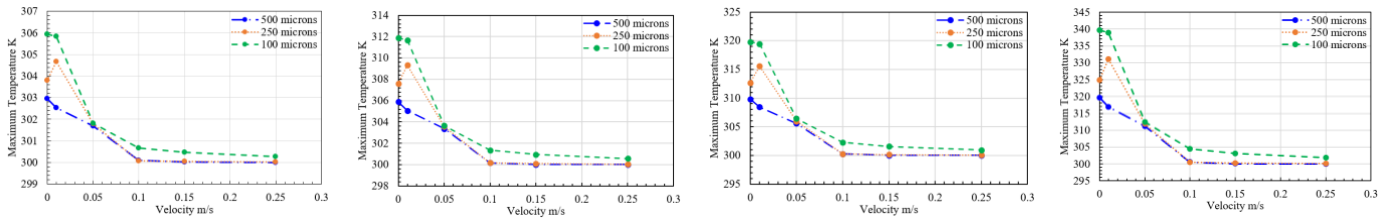

(a) (b) (c) (d)

Fig. 12: Maximum temperature of 100 µm, 250 µm, 500 µm solid particles based on various inlet velocities. ρ_p = 1500 kg/m^3. Working fluid = Water. Cylindrical ligament wall temperature T_{cw} = (a) 315 K (b) 330 K (c) 350 K (d) 400 K.

It is noteworthy that the highly complex and irregular nature of the metal foam ligaments means that the particles (unwanted solid materials) can deposit inside the metal foam structures. However, to reduce or eliminate this occurrence, there are two solutions. First, the MPM model will allow engineers to find out which metal foam properties (*i.e.* porosity, PPI, cell diameter, fibre diameter) are more susceptible to blocking of these solid particles. Then, engineers can use these results obtained from the MPM model to change the geometric morphology of metal foams with the aim to reduce or eliminate aggregation and deposition. This is the recommended step prior to large scale commercialization and deployment of the metal foam heat exchangers in environments where fouling is prevalent. The second approach is to use a suitable online and non-toxic antifouling technique that removes or eliminates aggregation and deposition in metal foam heat exchangers. This could be potentially achieved by using oscillatory pulsatile fluids which has shown to not only reduce time-averaged pressure drop but also reduce buildup of unwanted material (aggregation and deposition) in porous metal foam heat exchangers. This antifouling technique is covered extensively in a study by Kuruneru et al. (2018) and future studies entails studying the effects of fully resolved solid-fluid and solid-wall heat transfer coupled with oscillatory fluids.

7. Conclusions

A coupled finite volume (FVM) and macroscopic particle model (MPM) is developed to numerically investigate the pore-level analysis of non-isothermal solid-fluid flows through an idealized representation of a porous metal foam heat exchanger. The interaction between the particles and two different working fluids (air and water) and between the particles and the metal foam structure are investigated. One of the crucial aspects of this study is the development of a Macroscopic Particle Model (MPM) in ANSYS Fluent. The MPM model is used to assess the maximum temperature of various solid foulants under different operating conditions such as different inlet velocities. The numerical model is validated by comparing the numerical results pertaining to particle position, particle velocity, and Nusselt number against the experimental results. The maximum solid particle (foulant) temperature is found to be dependent on the

working fluid properties and particle properties. The highest foulant temperature is realized at low inlet velocities of metal foam heat exchangers. Critical inlet velocities where the maximum foulant temperature remains sensibly identical regardless of velocity is evaluated and differs based on the working fluid. Importantly, the presented numerical model permits engineers and scientists to reinforce the knowledge of multiphase non-isothermal solid-fluid flows through porous media and the coupled interphasic interactions between the solid-fluid and porous media. Secondly, this research serves as a steppingstone to undertake more complex analysis about heavy fouling in the form of particle deposition and particle aggregation coupled with heat transfer effects in porous heat exchangers.

Acknowledgements

The authors gratefully acknowledge the computational resources provided by UTS and in particular the ARClab (Advanced Research Computing Laboratory) run by the Faculty of Engineering and Information Technology (FEIT).

Conflict of interest

None declared.

References

Acmite, 2013. Global Heat Exchanger Market Report. Tech. Rep.

Afkhami, M., Hassanpour, A., Fairweather, M., & Njobuenwu, D. (2015). Fully coupled LES-DEM of particle interaction and agglomeration in a turbulent channel flow. Computers and Chemical Engineering, 78, 24-38

Ammar, Y. J. (2012). Low grade thermal energy sources and uses from the process industry in the UK. Applied Energy, 89(1), 3-20.

Bai, M., & Chung, J. (2011). Analytical and numerical prediction of heat transfer and pressure drop in open-cell metal foams. Int. J. of Thermal Sciences, 50, 869-880.

Banhart, J. (2000). "Manufacturing routes for metallic foams." The Journal of the Minerals **52**(12): 22-27.

Bayomy, A., Saghir, M., & Yousefi, T. (2016). Electronic cooling using water flow in aluminum metal foam heat sink: Experimental and numerical approach. International Journal of Thermal Sciences, 109, 182–200.

Bhattacharya, A. and R. Mahajan (2002). Numerical modeling of pressure drop across high porosity metal foams. 8th AIAA/ASME Joint Thermophysics and Heat Transfer Conference.

Bock, J., & Jacobi, A. M. (2013). Geometric classification of open-cell metal foams using X-ray micro-computed tomograhy. Materials Classification , 75, 35-43.

Boomsma, K., et al. (2003). "Simulations of flow through open cell metal foams using an idealized periodic cell structure." International Journal of Heat and Fluid Flow **24**(6): 825-834.

Buonomo, B., et al. (2016). A Numerical Analysis on a Compact Heat Exchanger in Aluminum Foam. Journal of Physics: Conference Series, IOP Publishing.

Chung, J., et al. (2006). Evaluation of open cell foam heat transfer enhancement for liquid rocket engines. 42nd AIAA/ASME/SAE/ASEE Joint Propulsion Conference & Exhibit.

Cui, H., Xu, F., Saha, S.C. (2015). “A three-dimensional simulation of transient natural convection in a triangular cavity.” International Journal of Heat and Mass Transfer, 85: 1012-1022.

Diani, A., et al. (2015). "Numerical investigation of pressure drop and heat transfer through reconstructed metal foams and comparison against experiments." International journal of heat and mass transfer **88**: 508-515.

Dukhan, N., et al. (2005). "One-dimensional heat transfer analysis in open-cell 10-ppi metal foam." International journal of heat and mass transfer **48**(25-26): 5112-5120.

Dukhan, N. (2006). "Correlations for the pressure drop for flow through metal foam."Experiments in Fluids **41**(4): 665-672.

Feng, Z.-G. and E. E. Michaelides (2005). "Proteus: a direct forcing method in the simulations of particulate flows." Journal of Computational Physics **202**(1): 20-51.

Feng, S., Kuang, J., Wen, T., Lu, T., & Ichimiya, K. (2014). An experimental and numerical study of finned metal foam heat sinks under impinging air jet cooling. International Journal of Heat and Mass Transfer, 77, 1063–1074.

Fluent, A. (2011). "ANSYS Fluent User's Guide." Ansys Inc.

Fuller, A. K. (2005). Measurement and interpretation of the heat transfer coefficients of metal foams. Proceedings of the Institution of Mechanical Engineers, Part C: Journal of Mechanical Engineering Science, 219(2), 183-191.

Ghosh, I. (2008). "Heat-transfer analysis of high porosity open-cell metal foam." Journal of heat transfer **130**(3): 034501.

Gondret, P., et al. (2002). "Bouncing motion of spherical particles in fluids." Physics of fluids **14**(2): 643-652.

Hooman, K. T. (2012). Impact of particulate deposition on the thermohydraulic performance of metal foam heat exchangers: A simplified theoretical model. Journal of Heat Transfer, 134(9), 92601.

Hosseini, S.B., et al. (2017). "Numerical study on polydisperse particle deposition in a compact heat exchanger." Applied Thermal Engineering **127**: 330-346.

John, D.A. (2011). Designing for comfort: selecting air-distribution outlets. ASHRAE J., 53(9), p.38

Krishnan, S., Hernon, D., Hodes, M., Mullins, J., & Lyons, A. (2012). Design of Complex Structured Monolithic Heat Sinks for Enhanced Air Cooling. IEEE Transactions on Components, Packaging and Manufacturing Technology, 2(2), 266–277.

Kuruneru, S.T.W., Sauret, E., Saha, S., & Gu, Y. (2016). Numerical investigation of the temporal evolution of particulate fouling in metal foams for air-cooled heat exchangers. Applied Energy, 184(C), 531–547.

Kuruneru, S.T.W., Sauret, E., Saha, S.C., Gu, Y.T. (2017a). Two- and four-way coupling of cohesive poly-disperse particulate foulants on a metal foam fiber immersed in quiescent fluid. International Communications in Heat and Mass Transfer, 89, 176-184

Kuruneru, S.T.W., Sauret, E., Vafai, K., Saha, S., & Gu, Y. (2017b). Analysis of particle-laden fluid flows, tortuosity and particle-fluid behaviour in metal foam heat exchangers. Chemical Engineering Science, 172(C), 677–687.

Kuruneru, S.T.W., Sauret, E., Saha, S., & Gu, Y. (2017c). A Novel Experimental Method to Assess Particle Deposition in Idealized Porous Channels. Heat Transfer Engineering, 38(11-12), 1008–1017.

Kuruneru, S.T.W., Sauret, E., Saha, S., & Gu, Y. (2018). Coupled CFD-DEM simulation of oscillatory particle-laden fluid flow through a porous metal foam heat exchanger: Mitigation of particulate fouling. Chemical Engineering Science, 179, 32–52.

Leong, K. and L. Jin (2005). "An experimental study of heat transfer in oscillating flow through a channel filled with an aluminum foam." International journal of heat and mass transfer **48**(2): 243-253.

Leong, K. and L. Jin (2006). "Effect of oscillatory frequency on heat transfer in metal foam heat sinks of various pore densities." International journal of heat and mass transfer **49**(3-4): 671-681.

Luo, K., et al. (2016). "Particle-resolved direct numerical simulation of gas–solid dynamics in experimental fluidized beds." AIChE Journal **62**(6): 1917-1932.

Mahdi, H., et al. (2006). "Thermal performance of aluminium-foam CPU heat exchangers." International journal of energy research **30**(11): 851-860.

Mahjoob, S., & Vafai, K. (2008). A synthesis of fluid and thermal transport models for metal foam heat exchangers. International Journal of Heat and Mass Transfer, 51(15-16), 3701–3711.

Mancin, S., et al. (2013). "Air forced convection through metal foams: Experimental results and modeling." International journal of heat and mass transfer **62**: 112-123.

Müller-Steinhagen, H., et al. (2011). Heat exchanger fouling: mitigation and cleaning strategies, Taylor & Francis.

Nawaz, K., Bock, J., & Jacobi, A., Thermal-hydraulic performance of metal foam heat exchangers under dry operating conditions. App. Thermal Eng., 119, 222–232.

Pan, H., et al. (2000). Experimental determination of effective heat conductivities of highly porous media. Industrial furnaces and boilers. European Conference.

Panchal, C. and E.-P. Huangfu (2000). "Effects of mitigating fouling on the energy efficiency of crude-oil distillation." Heat transfer engineering **21**(3): 3-9.

Pritchard, A. (1988). The economics of fouling. Fouling Science and Technology, Springer**:** 31-45.

Ranz, W. (1952). "Friction and transfer coefficients for single particles and packed beds." Chem. Eng. Prog. **48**: 247-253.

Saha, S.C., Patterson, J.C., Lei, C. (2011). "Scaling of Natural Convection of an Inclined Flat Plate: Sudden Cooling Condition" Journal of Heat Transfer 133(4), 041503.

Schampheleire, S., De Jaeger, P., Huisseune, H., Ameel, B., T'Joen, C., De Kerpel, K., & De Paepe, M. (2013). Thermal hydraulic performance of 10 PPI aluminium foam as alternative for louvered fins in an HVAC heat exchanger. Applied Thermal Engineering, 51(1-2), 371–382.

Seyf, H.R., & Layeghi, M. (2010). Numerical analysis of convective heat transfer from an elliptic pin fin heat sink with and without metal foam insert. J. of Heat Transfer, 132(7), 1-9.

Steinhagen, R., et al. (1993). "Problems and costs due to heat exchanger fouling in New Zealand industries." Heat transfer engineering **14**(1): 19-30.

Tamayol, A. and M. Bahrami (2008). Analytical determination of viscous permeability of fibrous porous media. ASME 2008 Fluids Engineering Division Summer Meeting collocated with the Heat Transfer, Energy Sustainability, and 3rd Energy Nanotechnology Conferences, American Society of Mechanical Engineers.

Tamayol, A. B. (2011). Transverse permeability of fibrous porous media. Physical Review E - Statistical, Nonlinear, and Soft Matter Physics, 83(4), 046314.

Thackery, P. (1980). "The cost of fouling in heat-exchange plant." Effluent & Water Treatment Journal **20**(3): 111-115.

Traore, P. L., Laurentie, J.C., & Dascalescu, L. (2015). An efficient 4 way coupling CFD-DEM model for dense gas-solid particulate flows simulations. Computers & Fluids, 113, 65-76

Wang, T. L., Luan, W., Liu, T., Tu, S.T., & Yan, J., Performance enhancement of thermoelectric waste heat recovery system by using metal foam inserts. Energy Conversion and Management, 124, 13-19.

Wang, F.-L., et al. (2017). "Real-time fouling characteristics of a typical heat exchanger used in the waste heat recovery systems." International journal of heat and mass transfer **104**: 774-786.

Zhang, H., et al. (2014). "Numerical investigation on the role of discrete element method in combined LBM–IBM–DEM modeling." Computers & Fluids **94**: 37-48.

Zhao, C. (2012). "Review on thermal transport in high porosity cellular metal foams with open cells." International journal of heat and mass transfer **55**(13-14): 3618-3632.

Zhi-Ming, X., et al. (2007). "Costs due to utility fouling in China."

Appendix

Table 8 MPM case studies

Inlet Velocity and Particle Initialization Velocity (m/s)						Particle Initial Temperature (K)	Particle density (kg/m^3)	Particle diameter (μm)	Fluid	Fluid Inlet Temperature (K)	Cylinder Wall Temperature (K)
0	0.01	0.05	0.1	0.15	0.25	300	1500	500	AIR	300	315
0	0.01	0.05	0.1	0.15	0.25	300	1500	500	AIR	300	330
0	0.01	0.05	0.1	0.15	0.25	300	1500	500	AIR	300	350
0	0.01	0.05	0.1	0.15	0.25	300	1500	500	AIR	300	400
0	0.01	0.05	0.1	0.15	0.25	300	1500	250	AIR	300	315
0	0.01	0.05	0.1	0.15	0.25	300	1500	250	AIR	300	330
0	0.01	0.05	0.1	0.15	0.25	300	1500	250	AIR	300	350
0	0.01	0.05	0.1	0.15	0.25	300	1500	250	AIR	300	400
0	0.01	0.05	0.1	0.15	0.25	300	1500	100	AIR	300	315
0	0.01	0.05	0.1	0.15	0.25	300	1500	100	AIR	300	330
0	0.01	0.05	0.1	0.15	0.25	300	1500	100	AIR	300	350
0	0.01	0.05	0.1	0.15	0.25	300	1500	100	AIR	300	400
0	0.01	0.05	0.1	0.15	0.25	300	1500	500	WATER	300	315
0	0.01	0.05	0.1	0.15	0.25	300	1500	500	WATER	300	330
0	0.01	0.05	0.1	0.15	0.25	300	1500	500	WATER	300	350
0	0.01	0.05	0.1	0.15	0.25	300	1500	500	WATER	300	400
0	0.01	0.05	0.1	0.15	0.25	300	1500	250	WATER	300	315
0	0.01	0.05	0.1	0.15	0.25	300	1500	250	WATER	300	330
0	0.01	0.05	0.1	0.15	0.25	300	1500	250	WATER	300	350
0	0.01	0.05	0.1	0.15	0.25	300	1500	250	WATER	300	400
0	0.01	0.05	0.1	0.15	0.25	300	1500	100	WATER	300	315
0	0.01	0.05	0.1	0.15	0.25	300	1500	100	WATER	300	330
0	0.01	0.05	0.1	0.15	0.25	300	1500	100	WATER	300	350
0	0.01	0.05	0.1	0.15	0.25	300	1500	100	WATER	300	400
0	0.01	0.05	0.1	0.15	0.25	300	8960 (Copper)	500	AIR	300	315
0	0.01	0.05	0.1	0.15	0.25	300	8960 (Copper)	500	AIR	300	400
0	0.01	0.05	0.1	0.15	0.25	300	8960 (Copper)	500	WATER	300	315
0	0.01	0.05	0.1	0.15	0.25	300	8960 (Copper)	500	WATER	300	400